RSC Advances

ROYAL SOCIETY OF CHEMISTRY

www.rsc.org/advances

Phenothiazine and pyridine-*N*-oxide based AIE-active triazoles: synthesis, morphology and photophysical properties

Dalila Belei[1], Carmen Dumea[1], Elena Bicu[1], Luminita Marin[2]*

[1] *"Alexandru Ioan Cuza" University, Department of Organic Chemistry, Iasi, Romania*

[2] *"Petru Poni" Institute of Macromolecular Chemistry of Romanian Academy, Iasi, Romania*

*email: lmarin@icmpp.ro

Abstract

Aggregation induced emission (AIE) low molecular weight compounds based on triazoles, phenothiazine and pyridine-*N*-oxide units bonded by short flexible chains have been obtained by a „click" chemistry reaction. The photophysical properties were explored by UV-vis and photoluminescence spectroscopy in solution, water suspension, amorphous and crystalline films. The UV-vis absorption spectra indicated a typical behavior for nanoparticle formation. An emission intensity enhancement of 233-fold higher was registered for the crystalline films compared to solutions, clearly indicating an aggregation induced emission behavior. The morphology study, in suspension and film, as monitored by dynamic light scattering, scanning electron microscopy and polarized light microscopy methods, indicated that nano- and micro- crystals in shape of rose-like and fibers were formed.

Keywords: triazole; phenothyazine; pyridine-*N*-oxide; aggregation induced emission; morphology

1. Introduction

Aggregation induced emission (AIE) is an intriguing optical phenomenon for which aggregation works constructively in light emission improving. Evidenced by Tang and its co-workers in 2001, it consists in emission appearance for aggregated compounds lacking of light emission in solution [1]. The AIE challenging phenomenon is quite opposite to the notorious aggregation caused quenching (ACQ) of light emission in the condensed phase, and comes in line with requirements of optoelectronic devices which need solid state emissive substrates. The signature of Tang group on AIE compounds is propeller-like design in which peripheral rigid aromatic units are linked by rotatable single bonds to a conjugated stator. This structural approach proved to facilitate the AIE effect because of the restricted-intramolecular rotation (RIR) [1], and a

large number of AIE compounds have been prepared based on this design, mainly using silole, tetraphenylethene, biphenyl based triazoles and so on [2]. In parallel, applying the RIR design, other groups started to work in this challenging domain, and the number and variety of AIE fluorogens increased constantly [2]. Tetraphenylethylene [3-5], carbazole [6], dicarbazolyl [7], maleimide [8], persulfurated benzene core [9], distyrylanthracene [10-12], binaphthyl [13], pyrrole, indole [14], pyridine [15], imine [16], metal complexis [17-19], PEG chains [20] were used as building blocks of numerous AIE active compounds, with practical applications biomedical field [21-24]. There are little results regarding AIE properties of phenothiazine containing compounds. Phenothiazine-hydrazone [25] or phenothiazine linked with anthracene groups [26, 27] or triarylamine [28] proved AIEE (aggregation induced enhanced emission) or AIE effect.

Phenothiazine based compounds have been intensely studied in the past decades due to their applications in the biological field in cancer therapy as photosensitizers for selective photodamage of cancer cells (photodynamic therapy) [29], or farnesyltransferase inhibitors [30], drugs for Alzheimer's disease [31] and so on. Also, these compounds have applications in electronic and optic devices as organic light emitting diodes [32], solar cells [33], chemical sensors [34]. Phenothiazine use in the active substrate of optoelectronic devices is based on its strong electron-donating character which promotes a good conjugation and therefore low band-gap with consequences upon charge carrier mobility improving and shifting in visible domain of light emission [35]. Moreover, due to the butterfly shape of phenothiazine fused ring, its derivatives preserve quite well the fluorescence quantum yield in solid state compared to solution [36]. However, as majority, the phenothiazine compounds luminescence is partially quenched in solid state compared to solution state – effect attributed to aggregation (ACQ).

The present paper describes the synthesis, self-assembling and optical properties of phenothiazine and pyridine-*N*-oxide based triazole compounds which exhibit AIE effect. All the structural blocks are biologically friendly units. Compared to already reported AIE compounds, their design distinguishes itself by the fact that small rigid units are linked by flexible spacers which assure a high mobility in solution and work to the self-assembling into ordered architectures [37].

2. Results and discussions

2.1. *Synthesis and structural characterization*

Three phenothiazine and pyridine-*N*-oxide based triazoles have been synthesised through „click" chemistry of pyridine-*N*-oxide carrying triple bond functionality with azide-containing phenothiazine. The intermediate pyridine-*N*-oxide carrying triple bond was prepared by the cycloaddition reaction of propargyl bromide with sodium 2-sulfidopyridine 1-oxide while the

intermediate azide was prepared from corresponding 10-chloroacetyl-10*H*-phenothiazine derivative and sodium azide using tetrabutylammonium bromide as phase transfer catalyst. The synthetic route to the target compounds (noted **5a**, **5b** and **5c**) is illustrated in Scheme 1. The molecular structure of the intermediates and final triazole compounds was confirmed by elemental analysis, ^{1}H- and ^{13}C-nuclear magnetic resonance (NMR) and Fourier transform infrared (FTIR) spectroscopic analysis.

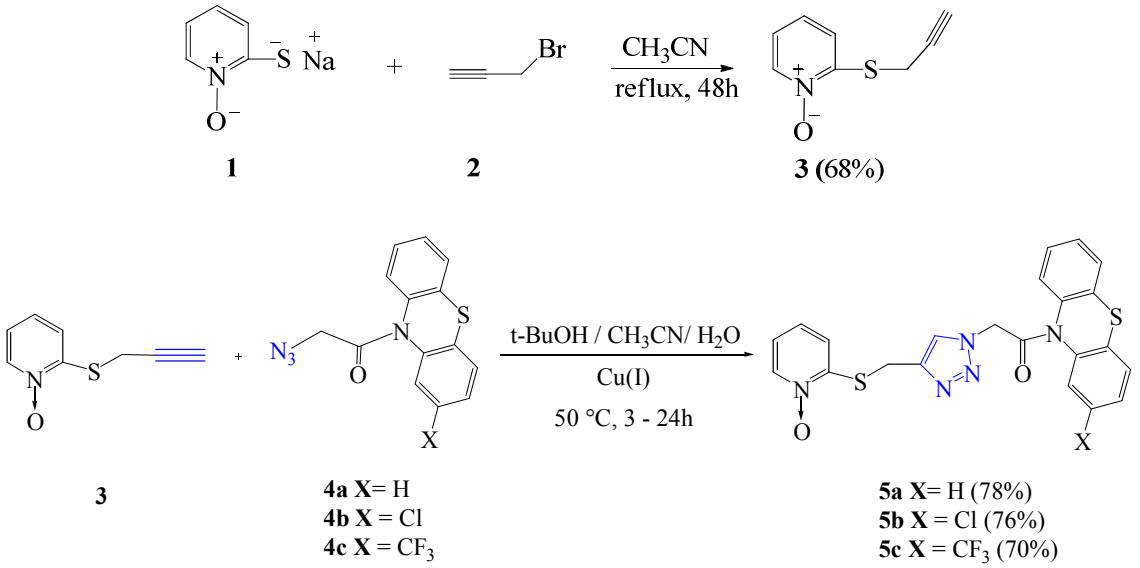

Scheme 1. Synthetic pathway to phenothiazine and pyridine-*N*-oxide based triazoles

In the FTIR spectra of the understudy triazoles, the stretching band characteristic to the H-C≡ units (3168 cm^{-1} and 2107 cm^{-1}) disappears, indicating the complete consumption of the triple bond during the cycloaddition reaction, whilst the triazole units are formed. All the other characteristic absorption bands of the synthesised compounds are present as well, confirming the right structure.

The ^{1}H- and ^{13}C-NMR spectra of the obtained compounds, further confirmed the target compounds, by the presence of all chemical shifts characteristic to protons and carbon atoms. The proton bands have the right coupling constants and integral ratio. The proton signal at 3.25 ppm attributed to the proton linked directly to the triple bond carbon is missing indicating its disappearance during the reaction, while the signal attributed to the sulfur neighbouring CH_2 protons (3.93 ppm) is shifted to higher frequency (4.33 ppm) reflecting the deshielding effect of the electron withdrawing triazole newly formed unit.

All the three samples (**5a**, **5b**, **5c**) were obtained in form of crystals, as was demonstrated by polarized optical microscopy (POM) observation. The **5a** sample exhibits birefringent grains, whilst

5b and **5c** samples show birefringent needles (Figure 1). The crystalline samples melt at high temperature and freeze in amorphous state during the cooling. The amorphous glass is stable in time as no crystallization was observed even after six months.

Figure 1. POM images of a) **5a**, b) **5b**, c) **5c** studied compounds, 40x10x2x magnification

The samples (**5a**, **5b**, **5c**) show good solubility in dimethylsulfoxide and poor solubility in other common organic polar solvents. They are completely insoluble in water and non-polar solvents.

2.2. *Photophysical properties*

UV-vis absorption

Photophysical properties of the studied triazoles were investigated in solution, suspension, amorphous and crystalline films. DMSO – a well known biocompatible dispersant [38], was used as solvent, whilst water – the principal component of the living organisms, was used as nonsolvent, so that premises for any possible biologic application were guaranteed. Due to their insolubility in water, the triazole molecules must aggregate in aqueous mixtures with high water fractions.

UV-vis absorption spectra of the triazole based compounds in THF or DMSO solution ($0.66x10^{-5}$ g/ml) show an identical trace profile consisting of three overlapping absorption maxima, corresponding to the π-π^* transition in the three isolated chromophore units of the dye molecules, with absorption edge around 344 nm (Figure 2a, Table 1). The wavelength of absorption light is relatively low because the flexible chains within the molecule structure hinder the extent conjugation. Different concentration of DMSO solutions shows variation of absorption intensity but no significant change in absorption maxima, suggesting the absence of significant ground state intermolecular interactions (Figure 2b).

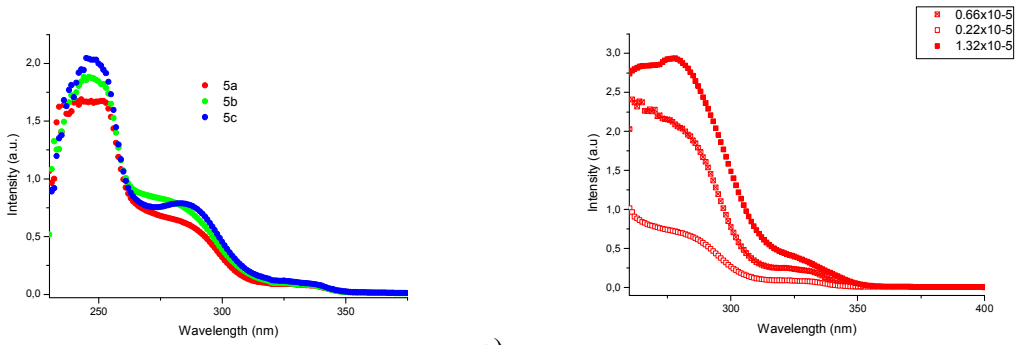

a) b)

Figure 2. UV-vis spectra of the a) triazole compounds in THF; b) compound **5a**, at different DMSO concentrations (inset: the concentration in g/mL)

The UV-vis spectra recorded for the DMSO-water solutions ($0.66x10^{-5}$ g/ml) in the same conditions showed drastic changes of the shape: the spectra intensity increases and their absorption edge is strong red shifted around 100 nm while the absorption band maxima are blue-shifted around 30 nm (Table 1) giving rise to a right tailed curve (Figure 3). The level-off tails at longer wavelength is attributed to the scattering effect of the nanoparticules obtained by chromophoric units aggregation in the water non-solvent [39]. The 30 nm blue shifting of absorption maximum is an unusual behaviour suggesting random twisted conformations, with worse conjugation [37, 40]. The comparison of the UV-vis spectra, in solution and water suspension (Figure 3b), suggests that dipolar aprotic DMSO solvent promotes planarization of the chromophore units by strong physical forces. By adding large amount of water, the hydrophobic dye molecules are constrained to segregate by self-assembling as nano/micro-aggregates. Within the aggregates, the chromophoric units adopt more twisted conformations because the absence of the strong polar solvent. The clearity of DMSO-water solutions showing no precipitates, clearly indicates macroscopically homogeneous solutions, sustaining the hypothesis of nano/micro sized aggregates.

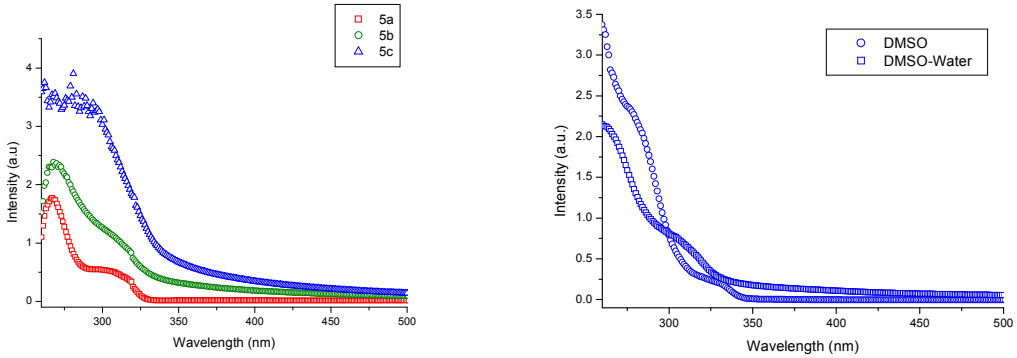

a) b)

Figure 3. UV-vis spectra a) of the samples in water DMSO-solutions and b) sample **5b** in DMSO and DMSO-water

The UV-vis spectra of the triazole compounds in solid state were registered for the films obtained in amorphous and crystalline state. The amorphous film spectra decreased in intensity and their absorption maxima are strong red-shifted (around 55 nm compared to DMSO solutions) – behaviour which reflects the chromophoric units planarization due to the reconformation by aggregation (Figure 4a) [41]. This is consistent with method of the films preparation – casting from DMSO solutions during a heating stage – which creates conditions for keeping the planarity of the chromophore π-conjugated units as gained in strong polar DMSO. It also favours a more tight packing of the molecules, and thus π-π* staking. In the absence of an extent conjugation (interrupted by the flexible chains) the strong red shift can be associated with intermolecular charge transfer transitions possibly originating from the excessive charge density of donor-acceptor pyridine-*N*-oxide chromophoric units [42]. Moreover, the presence of the triazole ring into the dye molecules provides additional possibilities for intermolecular charge transfer by H-bonding, π-π* stacking or donor-acceptor interactions [43].

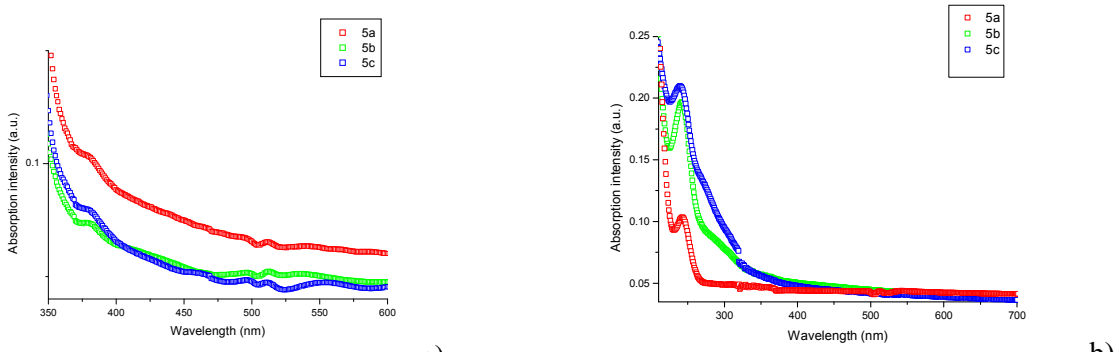

Figure 4. UV-vis spectra of the a) amorphous and b) crystalline film samples

On the contrary, the crystalline films casted from DMSO-water solution on glass substrate show a strong blue shifting of the absorption maxima (Figure 4b), suggesting twisted conformations that hinder the intermolecular charge transfer.

Table 1. UV-vis absorption maxima and absorption edge in solution, water suspension, amorphous and crystalline films

Code	λ_{max} (λ_{edge})/nm DMSO	λ_{max} (λ_{edge})/nm DMSO-H_2O	λ_{max} (λ_{edge})/nm amorphous film	λ_{max} (λ_{edge})/nm crystalline film
5a	259; 276; 325(344)	225; 258; 301(453)	379(577)	251(501)
5b	254; 277; 325(345)	221; 260; 302(467)	380(567)	250(497)
5c	248; 379; 324(344)	224; 257; 301 (449)	379(575)	251(487)

Comparing the absorption edge of the samples in all four diffrent states (Table 1), it can be seen a strong red shifting for the samples in suspension, amorphous and crystalline films compared to that in solutions, sugesting the formation of micro- / nano-sized aggregates.

Photoluminescence behaviour

The photoluminescence behaviour of the studied compounds, in solution, water suspension, as wel as amorphous and crystalline film, has been explored by exciting the samples at their absorption maxima wavelengths. The fluorescence intensity was calibrated using the Raman scatter peak of water [44].

The DMSO highly diluted solutions emit very weak intensity UV light, in the 350 – 375 nm wavelength domain, almost superposed with base line (Figure 5a, b). There is no influence of the exciting light wavelength on the emission profile, but the emission intensity increases when exciting light has lower wavelength. The Stokes shift has low values, indicating no significant geometrical rearrangements of the excited state [45]. As the sample solution was higly diluted ($0.66x10^{-5}$ g/mL) the emission effect could be attributed to the isolated species with no disturbance effect from the chromophoric interactions, and so by aggregate formation. Thus, the weak luminescence appears to be the result of dynamic intramolecular rotations which effectively consume the exciton energy of the chromophore units, and thus the molecules renders non-radiative.

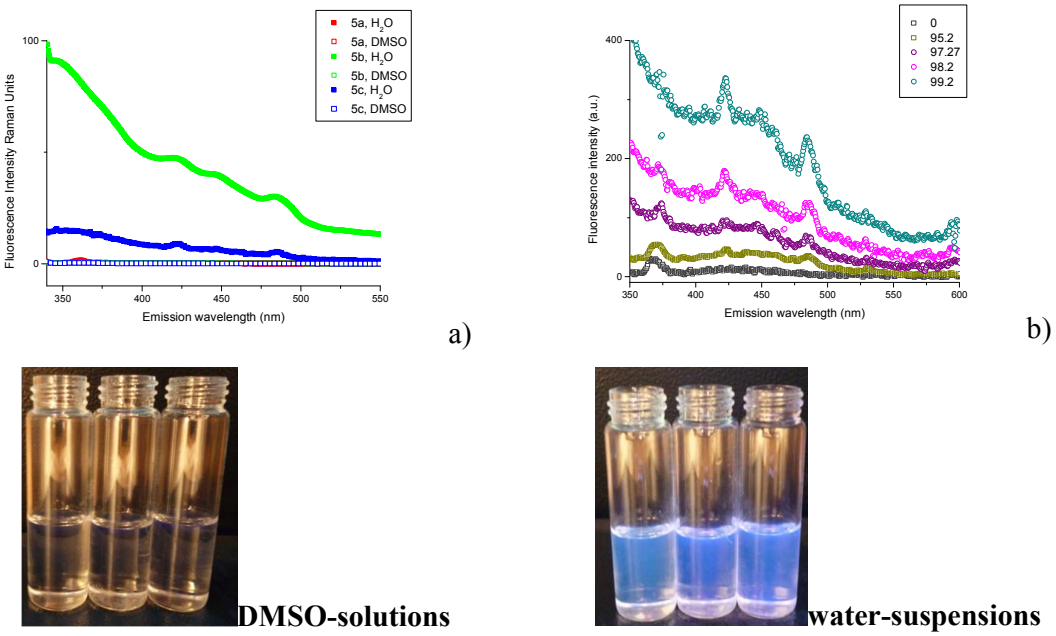

Figure 5. PL spectra of the triazoles a) DMSO-solutions and water-suspensions (the inset indicates the sample code and the solvent) and b) water suspension of **5c** sample ($0.66x10^{-5}$ g/mL) with different water fraction (the inset indicates the water fraction)

The situation completely changed in the case of water solutions, when all three samples emitted in a wide wavelength domain between 320 and 520 nm (Figure 5a, b). The prominent broad emission curve could be related to an increased number of molecular conformations appeared because of the free intramolecular rotation, allowed by the σ bonds between chromophoric rigid moieties. Mainly, the emission curve has three emission maxima, the most intense being in the UV domain. When illuminated with an UV lamp (360 nm), the solutions appear to have a weak violet-bluish luminescence. Compared to the DMSO solutions, the emission intensity in water suspension is 2-fold higher for sample **5a**, 48-fold higher for sample **5c** and 263-fold higher for sample **5b** (Table 2). The emission strengthening when water is added into DMSO solutions is attributed to the segregation of aggregates, accompanied by the physical constraint of the intramolecular rotations. As a consequence, the non- radiative channels are blocked, whilst the radiative ones are opened up. The segregation is possible because of the triazoles immiscibility with water which results in local increases of luminophore concentration. During the segregation process, the formation of aggregates with random structures is more probable owing to the large molecular conformation number which appears in DMSO solution. The random aggregates mitigate the π-π stacking interactions of the cromophoric units and thus excimer formation possibility. To better follow the influence of aggregation on the emission properties, the PL spectra were registered for aqueous mixtures with different water content. Figure 5b shows the water fraction dependent emission spectra of the sample **5c**, as an example. While the emission profile didn't show any changes until the water fraction (fw) reach 95 %, the emission intensity swiftly increases when the water content increases more and reaches a maximum for fw 99.2 %. This clearly indicating the aggregation induced emission. A similar behaviour was registered for the other samples.

Table 2. The light emission intensity of the studied triazoles*

Code	DMSO solution	DMSO-water suspension	Amorphous films	Crystalline films
5a	28	57.8	2483	6527
5b	35.5	9353	1544	6414
5c	34.5	1659	1301	5745

*calculated by integrating the calibrated emission curves [38]

For the amorphous film samples, the emission intensity increased more: 88, 43, and 37-fold higher in comparison to DMSO solutions (Table 2). The emission curves cover a large UV and visible domain, showing five overlapping emission bands with a maxim around 420 nm – corresponding to the violet-bluish light emission (Figure 6a). The multiple superposed emission bands confirm various motifs of self-assembling of the aggregates in various amounts, suggesting

various planarity degrees of the molecules. It is expected that the molecules, as a whole, to adopt twisted conformations in which planar chromophoric units inside molecules are tilted to one another under various angles. These random conformations promote different self-assembling motifs during slow DMSO evaporation, with longer or shorter intermolecular distances between fluorophoric units. The longer distances among fluorophoric units hinders the excimer and exciplex formation and cancels the non-radiative channels payable to π-π stacking, favoring the emission intensity increases.

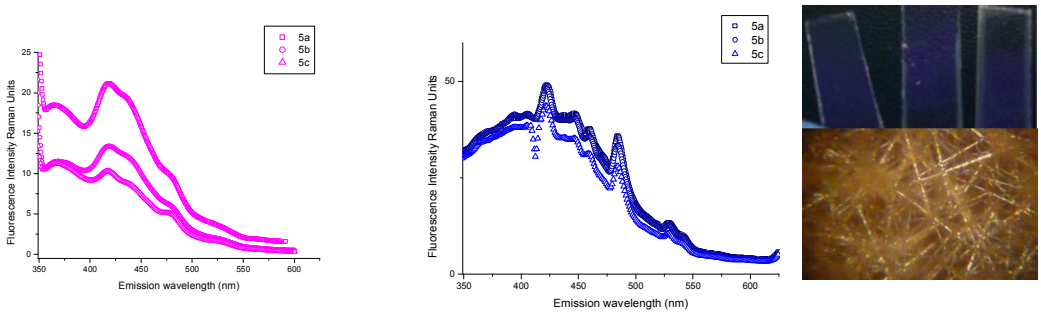

Figure 6. PL spectra of the a) amorphous and b) crystalline films; c) crystalline films of the **5a**, **5b**, **5c** under UV illuminating lamp and **5b** under polarized light

Compared to amorphous films, the crystalline ones casted from DMSO-water solution emit even more intense light, with the most intense emission maxima at 420 and 480 nm, both in the blue domain (Figure 6b). The emission intensity is 233-, 180- and 166-fold higher compared to the DMSO solution and 2.6-, 4.1- and 4.4-fold higher compared to the amorphous films (Table 2). The films show strong birefringence under polarized light and violet-bluish fluorescence when illuminated with un UV lamp (Figure 6c). The significant increases of the luminescence in crystalline state can be attributed to the increase of aggregate amount with longer intermolecular distances, prompted by the water non-solvent which forces the fast segregation and thus not allowing a close packing.

2.3. *Morphology*

To better understand the solvent influence on the optical behavior, especially to see the nano/micro aggregates formation, dynamic light scattering (DLS) on both types of solution samples (DMSO and DMSO-water) was performed. For the DMSO solution samples no nanoparticles were detected, which indicates that in this strong polar aprotic solvent, the molecules are dissolved as isolated species. The data completly changed for the DMSO-water solutions. The sample **5a** reveals typical spherical particles with hydrodynamic radius around 56.8 nm and PDI=0.59, indicating nanoparticle formation. The samples **5b** and **5c** exhibit a high aspect ratio corresponding to the

presence of nano- and micro-fibers (Table 3) [46]. DLS measurements allow us to make the suposition that in DMSO-water mixture, the studied compounds form fine suspensions despite their clear appearence.

Table 3. Diffusion light scattering on the water suspension samples

Code	Dimension (nm)	DPI
5a	56.8±14.5	0.59
5b	8733 ± 1673.4; 418.9 ± 39; 4395.2 ± 1150.3	2.434
5c	34.4 ± 10.1; 1148.5 ± 261.5; 18973.9 ± 5396.5	1.059

To have a visual confirmation of the nano-, micro-particle formation and their shape, scanning electron microscopy (SEM) of the samples obtained by casting DMSO-H_2O suspension on glass support has been performed. As can be seen in figure 7, the sample **5a** exhibits rose- like crystals, and **5b** and **5c** samples show entangled rod-like nano and micro-fibers forming networks.

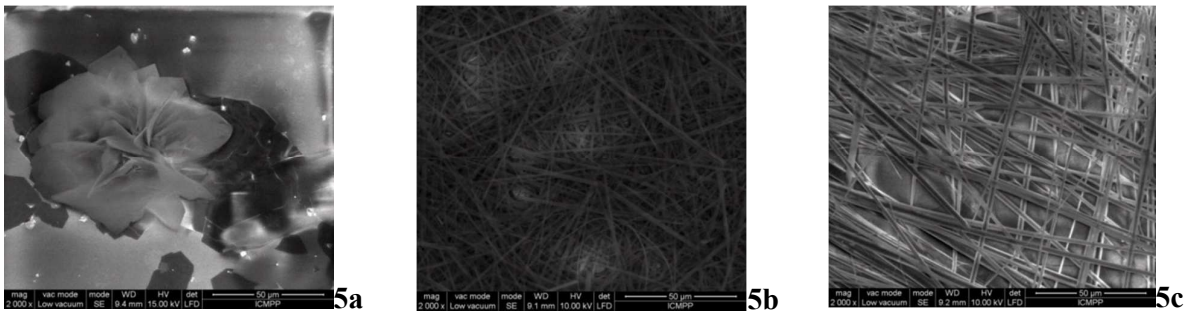

Figure 7. Scanning electron microphotographs of the studied samples

2.4. *Mechanism of aggregation induced emission*

Based on all the photophysical and morphological data collected, a scenario of aggregation induced emission of these flexible triazoles can be drawn.

In diluted solution, the flexible chains allow for active rotations of planar fluorophoric units (phenothiazine, pyridine-*N*-oxide, triazole). The intramolecular rotations serve as non-radiative channels for the excited states to decay, and on the other hand promote rich conformation variety. As a consequence, the aggregation occurs as result of two antagonistic features – structural flexibility and fluorophore planarity which promotes random aggregate formation with a variety of intermolecular distances, depending by the environment physical constraints and segregation time. Due to the large number of random conformers, the aggregation is driven by the flexibile units self-assembling, whilst the rigid units are packed in different conformations with intermolecular distances in different amounts. The short intermolecular distances within the fluorophore layers

facilitate the π-π interactions and thus favor the formation of excimers and exciplexis which quench the luminescence. On the other hand, the longer intermolecular distances are able to restrict the formation of detrimental excimers and exciplexis, and thus to block the non-radiative channels and to open up the radiative ones, leading to the observed AIE effect. Consequently, the emission intensity depends on the amount of larger intermolecular distances into aggregates. The amorphous films obtained from solutions favor a larger amount of shorter distances between the more planar fluorphoric units, whilst the crystalline films obtained from suspensions facilitate a larger amount of longer distances between fluorophoric units. This explains why crystalline films obtained from DMSO/water mixture with poor solvating power have better luminescence compared to amorphous films obtained from polar DMSO with high solvating power. On the other hand, it is expected that formation of nano- and micro-sized aggregates will enlarge emission surface, compared to the continuous amorphous glassy films and thus to further promote the enhancement of light emission intensity.

3. Experimental

3.1. Reagents

Propargyl bromide, sodium 2-sulfidopyridine 1-oxide, and phenothiazine were purchased from Aldrich and used without further purification. Solvents (CH_3CN, t-BuOH, THF, DMSO) were of high purities and used as purchased.

3.2. Equipments

IR spectra were recorded on a Bruker Tensor 27 – in reflectance mode, using a Gemini sampling accessory to collect horizontal attenuated total reflectance (ATR) spectra using a ZnSe crystal. IR spectra were recorded by accumulation of at least 64 scans, with a resolution of 2 cm^{-1}.

^{1}H and ^{13}C NMR spectra were recorded on a BRUKER Avance DRX 400 MHz spectrometer, equipped with a 5 mm direct detection QNP probe with z-gradients. The chemical shifts are reported as δ (ppm) relative to the residual peak of the DMSO solvent.

The particle size and size distribution were analyzed on a *dynamic light scattering* equipment Delsa Nano C, Beckman Coulter. The samples were prepared by dilution of the triazole compounds in pure DMSO or DMSO-H_2O mixture ($0.66x10^{-5}$ g/ml). The scattered light was measured at fixed angle 160°. The temperature was set at 25°±0.1 °C.

Scanning Electron Microscopy (SEM) images were aquired using Scanning Electron Microscope SEM EDAX – Quanta 200, at accelerated electron energy of 10 or 15 KeV. The samples were prepared by drop casting of water suspension solution on microscope glass. The solvent was evaporated in air, at room temperature.

The thermotropic behaviour of the triazole compounds was studied by observing the textures using an Olympus BH-2 *polarized light microscope* under cross polarizers with a THMS 600 hot stage and LINKAM TP92 temperature control system.

UV–Vis absorption and photoluminescence spectra were recorded on a Carl Zeiss Jena SPECORD M42 spectrophotometer and a Perkin Elmer LS 55 spectrophotometer, respectively, in solution and film, using 10 mm quartz cells and glass plates, respectively. The fluorescence intensity was calibrated using the Raman scatter peak of water [35]. The luminescence improving was calculated by integrating the emission bands.

The optical study in solution has been performed using stock solutions in DMSO. In order to confirm the absorption maxima, the UV-vis spectra were recorded in a wider wavelength domain, using solutions in THF, which has lower UV absorption than DMSO.

Determination of carbon, hydrogen, nitrogen and sulfur content of the compounds has been performed on a 2400 Series II CHNS Perkin Elmer elemental analyzer.

3.3.Synthesis

Three phenothiazine and pyridine-*N*-oxide based triazoles have been synthesised through „click" chemistry of pyridine-*N*-oxide carrying triple bond functionality and azide-containing phenothiazine (Scheme 1). Their synthesis is presented below.

Phenothiazine azides were synthesized in our laboratories, according to published procedures, as follows: 2-azido-1-(10*H*-phenothiazin-10-yl)ethanone [47], 2-azido-1-(2-chloro-10*H*-phenothiazin-10-yl)ethanone [48], and 2-azido-1-(2-(trifluoromethyl)-10*H*-phenothiazin-10-yl)ethanone [49].

2-(prop-2-yn-1-ylthio)pyridine-N-oxide

Propargyl bromide (12 mmoles) was added to a suspension of sodium 2-sulfidopyridine 1-oxide (10 mmoles) in 15 mL CH_3CN. The reaction mixture was stirred at reflux for 48 h. The resulting solid was collected by filtration, dried and recrystallized from ethanol to give pure 2-(prop-2-yn-1-ylthio)pyridine-*N*-oxide, as an ochre solid with a 68 % yield. mp 134-136 °C.

IR ν cm^{-1}: 3168 (νH-C≡), 2107 (νC≡C), 1588, 1553, 1472 (νC=C in aromatic rings), 1235 (νN→O), 1149 (ν pyridine), 836 (ν aromatic ring).

^{1}H NMR (DMSO-d_6, 400 MHz), δ(ppm): 8.33 (d, J = 6.4 Hz, 1H, Ar<u>H</u>); 7.41-7.49 (m, 2H, Ar<u>H</u>); 7.26 (dt, J = 8.6, 2.0 Hz, 1H, Ar<u>H</u>); 3.93 (d, J = 2.4 Hz, 2H, C<u>H</u>$_2$); 3.25 (t, J = 2.4 Hz, 1H, <u>H</u>-C≡).

^{13}C NMR (DMSO-d_6, 100 MHz), δ(ppm): 149.7 (<u>C</u>), 138.0 (<u>C</u>H), 125.4 (<u>C</u>H), 122.2 (<u>C</u>H), 121.4 (<u>C</u>H), 79.2 (<u>C</u>), 74.1 (<u>C</u>H), 17.7 (<u>C</u>H$_2$).

General procedure for the preparation of triazole derivatives

In a round bottom flask, a mixture of the azide (3 mmoles) and 2-(prop-2-yn-1-ylthio) pyridine-*N*-oxide (3 mmoles) was dissolved in a solvent mixture of *t*-BuOH and CH_3CN in volume

ratio 5:3. When the mixture cleared, a 10 % solution of sodium ascorbate (0.6 mmoli) and copper sulfate (0.3 mmoli) in water was added. The reaction mixture was kept under magnetic stirring at 50 °C for 3 – 24 h, as monitored by thin layer cromatography, and after which it was allowed to cool down to room temperature. In order to remove the inorganic salts, cold water and ammonium hydroxyde was added into the reaction flask. The resulting suspension was vigorously stirred at room temperature to complete the triazole precipitation and crude product was separated by filtration and finally washed with ethyl acetate to give pure 1,2,3-triazole derivatives.

2-[4-(1-Oxy-pyridin-2-ylsulfanylmethyl)-[1,2,3]triazol-1-yl]-1-phenothiazin-10-yl-ethanone: white solid, mp 242-245 °C, 78 % yield.

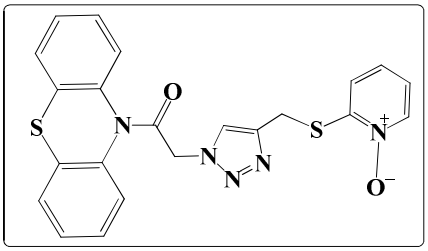

IR ν cm^{-1}: 1698 (ν N-C=O), 1579, 1552, 1472 (ν C=C in aromatic rings), 1260 (ν N→O), 1147 (ν pyridine), 759 (ν aromatic ring).

^{1}H NMR (DMSO-d_6, 400 MHz) δ(ppm): 8.30 (d, J = 6.0 Hz, 1H, ArH), 8.02 (s, 1H, ArH), 7.75 (broad signal, 1H, ArH), 7.60 (d, J = 7.6 Hz, 3H, ArH), 7.44 (t, J = 7.6 Hz, 2H, ArH), 7.33-7.38 (m, 3H, ArH), 7.21 (t, J = 6.4 Hz, 1H, ArH), 5.52 (broad signal, 2H, CH_2CO), 4.33 (s, 2H, CH_2S).

^{13}C NMR (DMSO-d_6, 100 MHz) δ(ppm): 164.7 (C), 150.3 (C), 142.2 (C), 138.0 (CH), 137.1 (2C), 132.2 (2C), 128.1 (CH), 127.6 (2CH), 127.0 (CH), 125.3 (2CH), 125.2 (2CH), 122.1 (2CH), 121.2 (2CH), 51.4 (CH_2), 24.3 (CH_2).

Elemental analysis calc. for C22H19N5O2S2 (449.5): C 58.78; H 4.26; N 15.58; O 7.12; S 14.26. Found: C 58.69; H 4.31; N 15.72; S 14.32.

1-(2-Chloro-phenothiazin-10-yl)-2-[4-(1-oxy-pyridin-2-ylsulfanylmethyl)-[1,2,3]triazol-1-yl]-ethanone: white solid, mp 237-240 °C, 76 % yield.

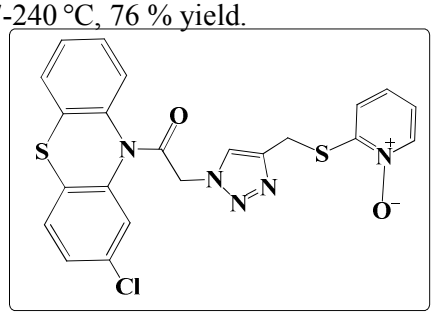

IR ν cm^{-1}: 1704 (ν N-C=O), 1575, 1554, 1471 (ν C=C in aromatic rings), 1247 (ν N→O), 1151 (ν pyridine), 754 (ν aromatic ring).

^{1}H NMR (DMSO-d_6, 400 MHz) δ(ppm): 8.30 (d, J = 6.0 Hz, 1H, ArH) 8.02 (s, 1H, ArH), 7.84 (broad signal, 1H, ArH), 7.76 (broad signal, 1H, ArH), 7.60-7.62 (m, 3H, ArH), 7.33-7.48 (m, 4H, ArH), 7.21 (t, J = 6.4 Hz, 1H, ArH), 5.61 (broad signal, 1H, CH_2), 5.53 (broad signal, 1H, CH_2CO), 4.33 (s, 2H, CH_2S).

^{13}C NMR (DMSO-d_6, 100 MHz) δ(ppm): 174.4 (C), 164.8 (C), 150.4 (C), 142.3 (C), 138.3 (C), 138.1 (CH), 136.5 (C), 131.8 (C), 131.4 (C), 129.2 (CH), 128.2 (CH), 127.8 (CH), 127.5 (CH), 127.0 (CH), 126.9 (CH), 125.3 (CH), 125.2 (CH), 122.1 (2CH), 121.2 (CH), 51.4 (CH_2), 24.3 (CH_2).

Elemental analysis calc. for C22H18ClN5O2S2 (484): C 54.6; H 3.75; Cl 7.3; N 14.4; O 6.6; S 13.2. Found: C 54.35; H 3.91; N 14.7; S 13.28.

2-[4-(1-Oxy-pyridin-2-ylsulfanylmethyl)-[1,2,3]triazol-1-yl]-1-(2-trifluoromethyl-phenothiazin-10-yl)-ethanone: white solid, mp 230-232 °C, 70 % yield.

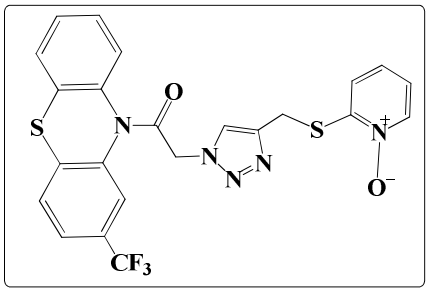

IR ν cm^{-1}: 1702 (ν N-C=O), 1551, 1470 (ν C=C in aromatic rings), 1245 (ν N→O), 1151 (ν pyridine), 763 (ν aromatic ring).

^{1}H NMR (DMSO-d_6, 400 MHz) δ(ppm): 8.30 (d, J = 6.4 Hz, 1H, ArH), 8.07 (s, 1H, ArH), 8.02 (s, 1H, ArH), 7.83 (d, J = 8.0 Hz, 1H, ArH), 7.70 (d, J = 8.4 Hz, 1H, ArH), 7.64 (d, J = 7.6 Hz, 1H, ArH), 7.60 (d, J = 8.4 Hz, 2H, ArH), 7.50 (t, J = 7.6 Hz, 1H, ArH), 7.41 (t, J = 7.6 Hz, 1H, ArH), 7.35 (t, J = 7.6 Hz, 1H, ArH), 7.20 (dt, J = 7.6, 1.6 Hz, 1H, ArH), 5.69 (broad signal, 1H, CH_2CO), 5.46 (broad signal, 1H, CH_2CO), 4.33 (s, 2H, CH_2S).

^{13}C NMR (DMSO-d_6, 100 MHz) δ(ppm): 165.0 (C), 150.4 (C), 142.3 (C), 138.1 (CH), 137.5 (C), 136.3 (C), 131.4 (C), 129.0 (2CH), 128.4 (CH), 128.1 (C), 128.0 (CH), 127.0 (CH), 125.3 (CH), 125.2 (CH), 125.1 (C), 124.1 (CH), 123.9 (CH), 122.4 (C), 122.1 (CH), 121.2 (CH), 51.3 (CH_2), 24.3 (CH_2).

Elemental analysis calc. for C23H18F3N5O2S2 (517.5): C 53.38; H 3.51; F 11.01; N 13.53; O 6.18; S 12.39. Found: C 53.19; H 3.56; N 13.60; S 12.43.

Sample preparation for AIE measurements

Stock solutions with a concentration of 1% w/v were prepared by dissolving 10 mg triazole in 1 mL DMSO. Parts of the stock solution were transferred into 10 mL vials and diluted with appropriate amounts of DMSO or water in order to obtain 0.66x10^{-5} g/mL solutions.

Film preparation by drop casting

Amorphous films have been prepared by drop casting 1% compound solution in DMSO on a glass support heated at 100 ^{o}C.

Ordered films, in form of micro- and nano-crystals have been prepared by drop casting a solution obtained by diluting 20 μL of 1% DMSO solution in 3mL water.

Conclusions

Three triazoles based on phenothiazine and pyridine-*N*-oxide units were prepared by "click" chemistry cycloaddition of pyridine-*N*-oxide carrying triple bond functionality and azide-containing phenothiazine. The small rigid structural blocks are linked together by short flexible units and were chosen to be biologically friendly. All three compounds exhibit aggregation induced emission phenomenon, with a 233-fold higher emission in crystalline state compared to solution, and with around 4-fold higher emission compared to amorphous state. The colour of emitted light is red shifted from UV light – in solution to bluish light – in water suspension and films. In solution and solid state, these compounds form nano- and micro- aggregates.

The increase in emission is in fact a consequence of restricted intramolecular rotations in solid state which prompts random self-assembling of the luminophore units, with large intermolecular distances, that mitigate stacking interactions and consequently open up the radiative chanels. The self-assembling of these units in nano- and micro- particles increase further the emission intensity of crystalline films *versus* amorphous ones.

The studied flexible triazoles studied in this paper draw attention to a new structural design in which small biologically friendly luminophore units are linked together by small flexible chains. This design enlarge the variety of the AIE luminogens based on the RIR mechanism to the flexible molecules, guiding further efforts in development of new AIE structures for appropriate applications, the biological ones being especially envisaged. The ability to emit light by aggregation in aqueous solutions can be used for designing contrast agents which can be further used for *in vivo* luminescence imaging of deep tissues for medical optical imaging.

Acknowledgements

The research leading to these results has received funding from the Romanian National Authority for Scientific Research, CNCS – UEFISCDI, project number PN-II-PT-PCCA-2013-4-1861 (contract number 272/2014).

One of the authors (Carmen Dumea) thanks for financial support of European Social Found within the Sectorial Operational Program Human Resources Development 2007 – 2013, through the Grant POSDRU/159/1.5/S/137750, ”Project Doctoral and Postdoctoral programs support for increased competitiveness in Exact Sciences research”.

Paper dedicated to the 65th anniversary of "Petru Poni" Institute of Macromolecular Chemistry of Romanian Academy, Iasi, Romania.

References

1. 1.Y. Hong, J.W.Y. Lam, B.Z. Tang, *Chem. Soc. Rev.*, 2011, **40**, 5361-5388.
2. Y. Hong, J.W.Y. Lam, B.Z. Tang, *Chem. Commun.*, 2009, 4332-4353.
3. R. Hu, J. W. Y. Lam, H. Deng, Z. Song, C. Zheng, B. Z. Tang, *Mater. Chem. C.*, 2014, **2**, 6326-6332.
4. M. Wang, G. Zhang, D. Zhang, D. Zhu, B. Z. Tang, *J. Mater. Chem.*, 2010, **20**, 1858-1867.
5. H. Tong, Y. Hong, Y. Dong, M. Häussler, Z. Li, J. W. Y. Lam, Y. Dong, H. H.-Y. Sung, I. D. Williams, B. Z. Tang, *J. Phys. Chem. B*, 2007, 111 (40), pp 11817-11823.
6. G. Tian, W. Huang, S. Cai, H. Zhou, B. Li, Q. Wanga, J. Su, *RSC Advances*, 2014, **4**, 38939-38942.
7. X. Zhang, Z. Chi, H. Li, B. Xu, X. Li, S. Liu, Y. Zhang, J. Xu, *Mater. Chem.*, 2011, **21**, 1788-1796.
8. M. Boominathan, V. Sathish, M. Nagaraj, N. Bhuvanesh, S. Muthusubramanian, S. Rajagopal, *RSC Advances*, 2013, **3**, 22246-22252.
9. A. Fermi, G. Bergamini, R. Peresutti, E. Marchi, M. Roy, P. Ceroni, M. Gingras, *Dyes Pigments*, 2014, **110**, 113-122.
10. X. Zhang, Z. Chi, B. Xu, L. Jiang, X. Zhou, Y. Zhang, S. Liu, J. Xu, *Chem. Commun.*, 2012, **48**, 10895-10897.
11. J. He, B. Xu, F. Chen, H. Xia, K. Li, L. Ye, W. Tian, *J. Phys. Chem. C.*, 2009, **113**, 9892-9899.
12. W. Guan, J. Lu, W. Zhou, C. Lu, *Chem. Commun.*, 2014, **50**, 11895-11898.
13. S. Sasaki, Y. Niko, K. Igawa, G. Konishi, *RSC Advances*, 2014, **4**, 33474-33477.
14. L. Marin, A. Zabulica, M.Sava, *Soft. Mater*., 2013, **11**, 32-39.
15. W-L. Chien, C-M. Yang, T-L. Chen, S-T. Li, J-L. Hong, *RSC Advances*, 2013, **3**, 6930-6938.
16. W. Luo, Y. Zhu, J. Zhang, J. He, Z. Chi, P.W. Miller, L. Chen, C-Y. Su, *Chem. Commun.*, 2013, **50**, 11942-11945.
17. X. Zhang, Z. Chi, Y. Zhang, S. Liu, J. Xu, *J. Mater. Chem. C.*, 2013, **1**, 3376-3390.

18. R. Yoshii, A. Nagai, K. Tanaka, Y. Chujo, *Chem. Eur. J.*, 2013, **19**, 4506-4512.
19. T. Yuan, R. T. K. Kwok, B. Z. Tang, B. Liu, *J. Am. Chem. Soc.*, 2014, **136**, 2546-2554.
20. X. Zhang, X. Zhang, B. Yang, S. Wang, M. Liu, Y. Zhang, L. Tao, Y. Wei, *RSC Advances*, 2013, **3**, 9633-9636.
21. X. Zhang, X. Zhang, L. Tao, Z. Chi, J. Xu, Y. Wei, *J. Mater. Chem. B*, 2014, **2**, 4398-4414.
22. D. Ding, K. Li, B. Liu, B. Z. Tang, *Acc. Chem. Res.*, 2013, 46, 2441–2453.
23. W. Ding, Y. Liu, Y. Li, Q. Shi, H. Li, H. Xia, D. Wang, X. Tao, *RSC Adv.*, 2014, **4**, 22651-22659.
24. M. Gao, C. K. Sim, C. W. T. Leung, Q. Hu, G. Feng, F. Xu, B. Z. Tang, B. Liu. *Chem. Commun.*, 2014, **50**, 8312-8315.
25. X. Cao, X. Zeng, L. Mu, Y. Chen, R-X. Wang, Y-Q. Zhang, J-X. Zhang, G. Wei, *Chem. J. Chinese U.*, 2012, **33**, 2084 – 2190.
26. M. Zheng, M. Sun, Y. Li, J. Wang, L. Bu, S. Xue, W. Yang, *Dyes Pigments,* 2014, **102**, 29-34.
27. X. Zhang, Z. Chi, J. Zhang, H. Li, B. Xu, X. Li, S. Liu, Y. Zhang, J. Xu, *J. Phys.Chem. B*, 2011, **115**, 7606-7611.
28. B. Wang, Y. Wang, J. Hua, Y. Jiang, J. Huang, S. Qian, H. Tian, *Chem. Eur. J.*, 2011, **17**, 2647-2655.
29. T-S. Hsieh, J-Y. Wu, C-C. Chang, *Chemistry*, 2014, **20**, 9709-15.
30. G-M. Dumitriu, A. Ghinet, E. Bicu, B. Rigo, J. Dubois, A. Farce, D. Belei, *Bioorg. Med. Chem. Let.*, 2014, **24**, 3180-3185.
31. A-L. Hui, Y. Chen, S-J. Zhu, C-S. Gan, J. Pan, A. Zhou, *Med. Chem. Res*., 2014, **23**, 3546-3557.
32. B. Kim, J. Lee, Y. Park, C. Lee, J.W. Park, *J. Nanosci. Nanotechno.*, 2014, **14**, 6404-6408.
33. G.A. Evtugyn, V.B. Stepanova, A.V. Porfireva, A.I. Zamaleeva, R.R. Fakhrullin, *J. Nanosci. Nanotechno.*, 2014, **14**, 6738-6747.
34. Y. Wu, H. Guo, X. Zhang, T.D. James, J. Zhao, *Chem. Eur. J.,* 2014, **17**, 7632-7644.
35. T. Duan, K. Fan, C. Zhong, W. Gao, X. Chen, T. Peng, J. Qin, *J. Photoch. Photobio. A*., 2014, **278**, 39-45.
36. A. Zabulica, M. Balan, D. Belei, M. Sava, B.C. Simionescu, L. Marin, *Dyes Pigments*, 2013, **96**, 686-698.
37. W.Z. Yuan, F. Mahtab, Y. Gong, Z-Q. Yu, P. Lu, Y. Tang, J.W.Y. Lam, C. Zhu, B.Z. Tang, *J. Mat. Chem.*, 2012, **22**, 10472-10479.
38. J.S. Kim, K.S. Song, J.H. Lee, I.J. Yu, *Arch. Toxicol.*, 2011, **85**, 1499-1508.
39. J. Wang, J. Mei, W. Yuan, P. Lu, A. Qin, J. Sun, Y. Ma, B.Z. Tang, *Chem. Mater*., 2011, **21**, 4056-4059.

40. Y-H. Lee,W-C Yen, W-F Suab, C-A Dai, *Soft Matter*, 2011, **7**, 10429-10442.
41. N. Kiriy, V. Bockarova, A. Kiriy, M. Stamm, F. C. Stamm, H. J. Adler, *Chem. Mater.* 2004, **16**, 4765-4771.
42. T. Biet, N. Avarvari, *Org. Biomol. Chem*., 2014, **12**, 3167-3174.
43. J. Shang, N.M. Gallagher, F. Bie, Q. Li, Y. Che, Y. Wang, H. Jiang, *J. Org. Chem*., 2014, **79**, 5134-5144.
44. J. Lawaetz, C.A. Stedman, *Appl. Spectrosc.* 2009, **63**, 936-940.
45. S. Mukherjee, P. Thilagar, *Chem. Eur. J.*, 2014, **20**, 8012-8023.
46. E.H. Qua, P.R. Hornsby, H.S.S. Sharma, G. Lyous. *J. Mater. Sci*., 2011, **46**, 6029-6045.
47. D. Belei, E. Bicu, P.G. Jones, M.L. Birsa, *J. Heterocyclic Chem.*, 2011, **48**, 129-134.
48. D. Belei, E. Bicu, M.L. Birsa, *Acta Chem. Iasi*, 2009, **17**, 197-207.
49. D. Addlaa, A. Jallapallya, D. Gurrama, P. Yogeeswarib, D. Sriramb, S. Kantevari, *Bioorg. Med. Chem. Lett.,* 2014, **24**, 233–236.